Nonlinear optical scattering: The concept of effective susceptibility

Sylvie Roke,[1,*] Mischa Bonn,[1,2] and Andrei V. Petukhov[3,*]
[1]*Leiden Institute of Chemistry, Leiden University, P.O. Box 9502, 2300 RA Leiden, The Netherlands*
[2]*FOM-Institute for Atomic and Molecular Physics, Kruislaan 407, 1098 SJ Amsterdam, The Netherlands*
[3]*Debye Institute, Utrecht University, P.O. Box 80051, 3508 TB Utrecht, The Netherlands*
(Received 3 February 2004; revised manuscript received 28 April 2004; published 17 September 2004)

We present a general theoretical method for deriving effective susceptibilities for (non)linear optical scattering processes of arbitrary order using the reciprocity principle. This method allows us to formulate a generalized treatment of nonlinear optical scattering and deduce selection rules independent of the precise mechanism of light-matter interaction. We particularize this approach to second-order sum frequency scattering from an inhomogeneous medium and consider the limiting cases of small particle scattering, refractive index matched (Rayleigh-Gans-Debye) scattering, small refractive index contrast (Wentzel-Kramers-Brillouin) scattering and correlated scattering. We compare the derived expressions to experimental results of sum frequency scattering from monodisperse particles in suspension with varying sizes.

DOI: 10.1103/PhysRevB.70.115106 PACS number(s): 82.70.Dd, 42.65.−k, 68.60.−p, 78.68.+m

I. INTRODUCTION

Nonlinear optical techniques have become well established tools to study the properties of various media.[1] Bulk sum- and difference frequency generation are often used to investigate the molecular properties of solids.[2] Even-order optical techniques like sum frequency generation[1] and five wave mixing[3–6] are very well suited to study the physical and chemical properties of interfaces. One of the key elements of these approaches is the coherent character of the detected light, which limits these techniques to the study of macroscopically flat surfaces. Only recently, attempts have been made to expand these surface specific techniques to investigate the properties of nonplanar surfaces, in particular to particles dispersed in dilute suspensions.[7–10]

Theoretically, several studies have been performed with the aim of modelling the radiation emitted in a nonlinear scattering event. These studies include second harmonic scattering from small dielectric[8,11] and metallic[12,13] spheres, from an ordered lattice[14] and from a small metallic hemispherical boss.[15] All of these investigations are aimed at finding a model for second harmonic generation (SHG) scattering from a typical—mostly spherical—particle shape. No description exists of a general scattering event of arbitrary order from an arbitrary shaped particle.

Previously, we have experimentally demonstrated the development of a novel molecular specific technique of sum frequency scattering.[9] This can result in access to a wealth of information on the physico-chemical molecular properties of the surfaces of vesicles, micelles and nanoparticles. In this paper, we introduce the concept of effective susceptibility for a (non)linear scattering event of arbitrary (*n*th) order from the reciprocity principle, which provides a general theoretical framework for nonlinear-optical scattering. This enables us to derive selection rules for different experimental geometries based on symmetry arguments alone. We then consider different limiting cases for sum frequency generation (SFG) scattering, for which appropriate assumptions exist. In particular we will consider small particle scattering, index matched (nonlinear Rayleigh-Gans-Debye) scattering, small contrast (nonlinear Wentzel-Kramers-Brillouin) scattering and correlated scattering. Finally, we will compare the results of the nonlinear Rayleigh-Gans-Debye (RGD) and Wentzel-Kramers-Brillouin (WKB) approximations with infrared-visible SFG scattering experiments from submicron sized colloids in suspension.

II. THEORY

The nonlinear response of a material to incident electromagnetic waves is usually described in terms of the nonlinear polarization. The polarization is related to the incoming field(s) by the nonlinear susceptibility $\vec{\vec{\chi}}$. Consequently, the susceptibility is a measure of how much polarization is built up in the medium by the incident fields. The incoming fields are considered to be composed of monochromatic plane waves of the form:

$$\mathbf{E}_{\alpha}^{\mathbf{k}}(\mathbf{r},t) = \mathcal{E}\mathbf{u}_{\alpha}e^{i(\mathbf{k}\cdot\mathbf{r}-\omega t)} \tag{1}$$

with $\mathcal{E}$ the scalar amplitude of the wave and $\mathbf{u}_{\alpha}$ the unit polarization vector (α denotes the polarization state). This restriction limits the further applicability to beams with a low intensity gradient in the beam waist, i.e. excludes tightly focused pulses as in Refs. 16 and 17. As the fields interact with the medium, there are two effects that modify the build-up of the local nonlinear polarization: a microscopic local field correction due to dipole-dipole interactions, and a change in the average macroscopic field due to the linear optical properties of the medium (see Ref. 15, and references therein). The first can be taken into account by the local Lorentz-Lorenz correction,[18] which we will not take into account in this description (but can be readily done). The latter can be

implemented by using Fresnel-type coefficients $\mathcal{L}_\alpha(\mathbf{r})$, which describe the modification of the local field by the particle (note that far from the particle $\mathcal{L}_\alpha(\mathbf{r}) \rightarrow \mathbf{u}_\alpha$), so that the local field becomes

$$\mathbf{E}_\alpha^{\mathbf{k}}(\mathbf{r},t) = \mathcal{E}\mathcal{L}_\alpha(\mathbf{r}) e^{i(\mathbf{k}\cdot\mathbf{r}-\omega t)}. \tag{2}$$

The most general form of the non-locally-induced nonlinear polarization reads as[1]

$$\mathbf{P}^{\omega_0=\omega_1+\ldots+\omega_n}(\mathbf{r}) = \int \cdots \int \vec{\vec{\chi}}(\mathbf{r},\mathbf{r}_1,\cdots,\mathbf{r}_n)\cdot\mathbf{E}^{\omega_1}(\mathbf{r}_1)\cdots\cdot\mathbf{E}^{\omega_n}(\mathbf{r}_n)d^3\mathbf{r}_1\cdots d^3\mathbf{r}_n, \tag{3}$$

which also includes any possible interaction with the magnetic field of the optical waves.[19] In particular, this allows us to set the optical magnetic permeability $\mu(\omega)\equiv 1$ without loss of generality in the following. Apart from assuming plane waves, we also restrict ourselves to detection in the far field. No other restriction (e.g., on the nature of light-matter interaction) is assumed in this section.

A. Reciprocity

Consider two different current sources $\mathbf{j}_1(\mathbf{r})$ and $\mathbf{j}_2(\mathbf{r})$ emitting optical fields $\mathbf{E}_1$ and $\mathbf{E}_2$ at a single frequency. Then the relationship between the currents $\mathbf{j}_{1,2}$ and the fields $\mathbf{E}_{1,2}$ is given by the following relation[19]

$$\int \mathbf{j}_1(\mathbf{r})\cdot\mathbf{E}_2(\mathbf{r})d^3\mathbf{r} = \int \mathbf{j}_2(\mathbf{r})\cdot\mathbf{E}_1^\dagger(\mathbf{r})d^3\mathbf{r}, \tag{4}$$

where the integrals are taken over the volumes of the sources and the † denotes that all nonreciprocal interactions must be reversed in the calculation of the radiated field $\mathbf{E}_1^\dagger(\mathbf{r})$ (see Ref. 20). Equation (4) is known as the reciprocity theorem and is one of the basic concepts in physics. In linear optics reciprocity arises from the following (Onsager) symmetry of the linear susceptibility[20]

$$\vec{\vec{\chi}}_{ij}(\mathbf{r},\mathbf{r}_1) = \vec{\vec{\chi}}_{ji}^{\,\dagger}(\mathbf{r}_1,\mathbf{r}), \tag{5}$$

where $\vec{\vec{\chi}}^\dagger$ is the susceptibility of the same medium after application of the time-inversion operation. The application of the time-inversion operation is relevant for example, in magnetic materials where it reverses the direction of the dc media magnetization. In nonmagnetic media, which can be described by a local dielectric response, this leads to a symmetric dielectric response tensor $\vec{\vec{\epsilon}}_{ij}(\mathbf{r}) = \vec{\vec{\epsilon}}_{ji}(\mathbf{r})$. Note that light absorption, which is an intrinsically nonreversible process, does not affect the reciprocity. The Onsager symmetry [Eq. (5)] yields a general relation between results of two experimental situations, in which the position of a monochromatic light source and a detector are exchanged.[19–22]

As the current and polarization are related by $\mathbf{j}=(\partial\mathbf{P}/\partial t)$, the reciprocity theorem can be used to describe (non)linear-optical scattering from a particle. One can consider the two situations that are sketched in Fig. 1. In the first we are dealing with a current source ($\mathbf{j}_1$) induced in the scattering particle by an *n*th order nonlinear optical interaction with *n* incoming waves that emits a field $\mathbf{E}_1$ which is detected at position $\mathbf{r}_0$. In the second situation we are dealing with a dipolar point source located at $\mathbf{r}_0$ having a current $\mathbf{j}_2 \sim \delta(\mathbf{r}-\mathbf{r}_0)$ that induces a field $\mathbf{E}_2$ in the particle.

Assuming that the detector is placed in the Fraunhofer zone, the wave incident from the detector on the particle can be treated as a plane wave. Knowing the relation between $\mathbf{j}_2$ and the distribution of the local field $\mathbf{E}_2(\mathbf{r})$ it induces in the particle, we can employ the reciprocity theorem, Eq. (4), to evaluate the field $\mathbf{E}_1$ at the detector position, which can have two orthogonal polarization components. To calculate its amplitude $\mathcal{E}_{\alpha_0}^{\mathbf{k}_0}$ in a given polarization state α_0, one has to choose the direction of $\mathbf{j}_2$ along the polarization vector. Here $\mathbf{k}_0$ denotes the wave vector of the wave scattered into the direction of the detector. Thus, the calculation of the emitted field is now transformed into the problem of finding the local field distribution induced by a plane wave of frequency ω_0. The result can be written in the form

$$\mathcal{E}_{\alpha_0}^{\mathbf{k}_0} = e^{ik_0 r_0}\frac{k_0^2}{r_0}\Gamma_{\alpha_0,\alpha_1,\cdots,\alpha_n}^{\mathbf{k}_0,\mathbf{k}_1,\cdots,\mathbf{k}_n}\mathcal{E}_{\alpha_0}^{\mathbf{k}_0}\mathcal{E}_{\alpha_1}^{\mathbf{k}_1}\cdots\mathcal{E}_{\alpha_n}^{\mathbf{k}_n}. \tag{6}$$

Here $\alpha_1,\ldots,\alpha_n$ and $\mathbf{k}_1,\ldots,\mathbf{k}_n$ denote the polarization state and the wave vectors of the incident plane waves and

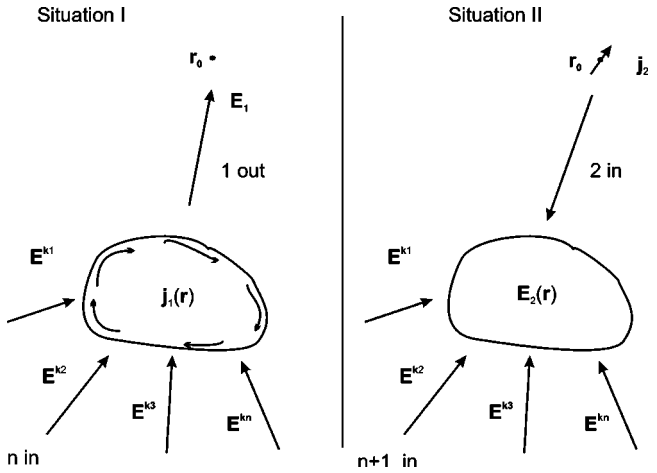

FIG. 1. Two different current sources. Current source 1 is the scattering object (with the center of mass placed at the origin), in which the currents are induced by an *n*th order nonlinear optical interaction. $\mathbf{E}_1$ is the field measured by a detector at $\mathbf{r}_0$. Current source 2 is a point dipole. $\mathbf{E}_2$ is the field experienced by the particle.

$$\Gamma^{\mathbf{k}_0,\mathbf{k}_1,\ldots,\mathbf{k}_n}_{\alpha_0,\alpha_1,\ldots,\alpha_n} = \int\int\cdots\int \mathcal{L}^{-\mathbf{k}_0,\dagger}_{\alpha_0}(\mathbf{r})\cdot\vec{\vec{\chi}}(\mathbf{r},\mathbf{r}_1,\ldots,\mathbf{r}_n)\cdot\mathcal{L}^{\mathbf{k}_1}_{\alpha_1}(\mathbf{r}_1)\cdots\mathcal{L}^{\mathbf{k}_n}_{\alpha_n}(\mathbf{r}_n)e^{i(-\mathbf{k}_0\cdot\mathbf{r}+\mathbf{k}_1\cdot\mathbf{r}_1\cdots\mathbf{k}_n\cdot\mathbf{r}_n)}d^3\mathbf{r}\ d^3\mathbf{r}_1\cdots d^3\mathbf{r}_n \tag{7}$$

can be interpreted as an effective nonlinear polarizability of the scattering object. It is analogous to atomic or molecular polarizability, which is often introduced to describe the nonlinear-optical interactions in, e.g., gases with the exception that $\Gamma^{\mathbf{k}_0,\mathbf{k}_1,\cdots,\mathbf{k}_n}_{\alpha_0,\alpha_1,\cdots,\alpha_n}$ is not only a property of the scattering object, but also depends on the experimental geometry via the wave vectors $\mathbf{k}_0,\mathbf{k}_1,\ldots,\mathbf{k}_n$ of the interacting waves. In its essence, this treatment replaces an extended scattering object, which could have any complex internal structure with any nature of internal nonlinear interaction, by a simple point object with dipole nonlinear polarizability given by Eq. (7) that creates exactly the same scattered field at the position of the detector for a given experimental configuration.

Thus, the reciprocity theorem allows us to reformulate the problem in a way that is symmetric with respect to the incident and outgoing fields. This intrinsic symmetry of Eq. (7) ensures reciprocity on the level of the field scattered by the whole particle. One can also show that this symmetry is needed in nonabsorbing systems to ensure energy conservation and the Manley-Rowe relations[23] requiring that equal amount of photons are emitted into or absorbed from each interacting wave.

B. Symmetry

In nonlinear optics one often applies symmetry arguments on the level of the susceptibility $\vec{\vec{\chi}}$. The effective susceptibility presented in Eq. (7) is an integrated quantity, which is not a function of the scattering object alone, but also depends on the experimental geometry via the wave vectors $\mathbf{k}_i$. Still, one can apply the symmetry operations to the whole scattering geometry.[24] Thus, particle symmetry (like, e.g., inversion symmetry) is no longer the sole factor of relevance. This allows us to directly formulate selection rules for different scattering events, independent of the mechanisms of linear- and nonlinear-light-matter interactions.

For example, when using a planar geometry, (i.e., all incident and scattered beams lie within one (scattering) plane), the polarization direction of the waves parallel (perpendicular) to that plane are defined as $p(s)$. If the particle is symmetric with respect to the scattering plane, then, upon reflection in the symmetry plane all p-polarized waves and $\vec{\vec{\chi}}$ remain unchanged, whereas the s-polarized waves change phase by a factor of π. The induced polarization should be the same for both cases. Hence for all nth order scattering processes all elements of $\vec{\vec{\Gamma}}^{\mathbf{k}_0,\mathbf{k}_1,\ldots,\mathbf{k}_n}_{\alpha_0,\alpha_1,\ldots,\alpha_n}$ with an odd number of s-polarized waves must equal 0. Thus, in the case of in-plane second-order scattering there are only four allowed elements of $\vec{\vec{\Gamma}}^{\mathbf{k}_0,\mathbf{k}_1,\mathbf{k}_2}_{\alpha_0,\alpha_1,\alpha_2}$ (*ppp*, *ssp*, *sps*, and *pss*). Analogously, for third-order scattering there are only 8 allowed elements of $\vec{\vec{\Gamma}}^{\mathbf{k}_0,\mathbf{k}_1,\mathbf{k}_2,\mathbf{k}_3}_{\alpha_0,\alpha_1,\alpha_2,\alpha_3}$, (*ssss*, *pppp*, *sspp*, *ppss*, *spsp*, *psps*, *pssp*, and *spps*). For situations with an additional twofold rotational symmetry (which is the case in second harmonic scattering, when detection is in the forward, or backward direction) no even-harmonic scattering can occur as the only allowed elements must have both an even number of s- and p-polarized waves. This symmetry is broken if one uses noncollinear input waves of different frequencies (which occurs for example in infrared-visible sum frequency generation).

III. SUM FREQUENCY SCATTERING

The solutions to Eqs. (6) and (7) for the scattered fields depend on the order of the scattering event and on possible simplifications imposed by the symmetry of the geometry. In the following description we focus on second-order scattering processes. For dielectric and metallic *spherical* particles an exact treatment (Mie theory) exists for second harmonic scattering, in which the amplitude of the scattered wave is expressed as a set of absolutely converging series of complex terms, which involve spherical harmonics and Bessel functions of increasing order.[8,12] For the special case of second-order sum frequency scattering the effective susceptibility [(Eq. (7))] becomes:

$$\Gamma^{\mathbf{k}_0,\mathbf{k}_1,\mathbf{k}_2}_{\alpha_0,\alpha_1,\alpha_2} = \int \mathcal{L}^{-\mathbf{k}_0,\dagger}_{\alpha_0}(\mathbf{r})\cdot\vec{\vec{\chi}}(\mathbf{r},\mathbf{r}_1,\mathbf{r}_2)\cdot\mathcal{L}^{\mathbf{k}_1}_{\alpha_1}(\mathbf{r}_1)\cdot\mathcal{L}^{\mathbf{k}_2}_{\alpha_2}(\mathbf{r}_2)e^{i(-\mathbf{k}_0\cdot\mathbf{r}+\mathbf{k}_1\cdot\mathbf{r}_1+\mathbf{k}_2\cdot\mathbf{r}_2)}d^3\mathbf{r}d^3\mathbf{r}_1d^3\mathbf{r}_2. \tag{8}$$

We will use this expression as a starting point for sum frequency scattering from small particles (Sec. III A). In Secs. III B and III C we will implement approximations that are generally employed in nonlinear surface spectroscopy.

A. Small particles

To consider the scattering from small particles (with size dimension σ) we decompose the local-field factors into even and odd parts as

$$\mathcal{L}_{\alpha}^{\mathbf{k}}(\mathbf{r}) = \mathcal{L}_{\alpha}^{\mathbf{k},\mathrm{even}}(\mathbf{r}) + \mathcal{L}_{\alpha}^{\mathbf{k},\mathrm{odd}}(\mathbf{r}), \tag{9}$$

where

$$\mathcal{L}_{\alpha}^{\mathbf{k},\mathrm{even}}(\mathbf{r}) \equiv \tfrac{1}{2}(\mathcal{L}_{\alpha}^{\mathbf{k}}(\mathbf{r}) + \mathcal{L}_{\alpha}^{-\mathbf{k}}(\mathbf{r})), \tag{10}$$

$$\mathcal{L}_{\alpha}^{\mathbf{k},\mathrm{odd}}(\mathbf{r}) \equiv \tfrac{1}{2}(\mathcal{L}_{\alpha}^{\mathbf{k}}(\mathbf{r}) - \mathcal{L}_{\alpha}^{-\mathbf{k}}(\mathbf{r})), \tag{11}$$

where $\mathcal{L}_{\alpha}^{\mathbf{k}}$ and $\mathcal{L}_{\alpha}^{-\mathbf{k}}$ are the normalized local fields of the wave, propagating in the forward and backward directions.

The interactions are now split into a centrosymmetric [Eq. (10)] and an anticentrosymmetric part [Eq. (11)]. Expanded in powers of σ/λ, the lowest order contribution to $\mathcal{L}_{\alpha}^{\mathbf{k},\mathrm{even}}(\mathbf{r})$ comes from $(\sigma/\lambda)^0$. Likewise $\mathcal{L}_{\alpha}^{\mathbf{k},\mathrm{odd}}(\mathbf{r})$, is determined by $(\sigma/\lambda)^1$.

If we expand the phase factors in Eq. (7) as well, we can decompose the effective susceptibility [Eq. (7)] in powers of σ/λ. The zeroth-order contains all even parts of the local field

$$\Gamma_{\alpha_0,\alpha_1,\alpha_2}^{\mathbf{k}_0,\mathbf{k}_1,\mathbf{k}_2} = \int \mathcal{L}_{\alpha_0}^{\mathbf{k}_0,\mathrm{even},\dagger} \cdot \vec{\vec{\chi}}(\mathbf{r},\mathbf{r}_1,\mathbf{r}_2) \cdot \mathcal{L}_{\alpha_1}^{\mathbf{k}_1,\mathrm{even}}(\mathbf{r}_1) \cdot \mathcal{L}_{\alpha_2}^{\mathbf{k}_2,\mathrm{even}}(\mathbf{r}_2) d^3\mathbf{r}\, d^3\mathbf{r}_1 d^3\mathbf{r}_2. \tag{12}$$

The next order in (σ/λ) is obtained by expanding the phase factor in Eq. (8) or by using the odd part for one of the local fields yielding:

$$\begin{aligned}
\Gamma_{\alpha_0,\alpha_1,\alpha_2}^{\mathbf{k}_0,\mathbf{k}_1,\mathbf{k}_2} = & \int \mathcal{L}_{\alpha_0}^{-\mathbf{k}_0,\mathrm{even},\dagger}(\mathbf{r}) \cdot \vec{\vec{\chi}}(\mathbf{r},\mathbf{r}_1,\mathbf{r}_2) \cdot \mathcal{L}_{\alpha_1}^{\mathbf{k}_1,\mathrm{even}}(\mathbf{r}_1) \cdot \mathcal{L}_{\alpha_2}^{\mathbf{k}_2,\mathrm{odd}}(\mathbf{r}_2) d^3\mathbf{r}\, d^3\mathbf{r}_1 d^3\mathbf{r}_2 \\
& + \int \mathcal{L}_{\alpha_0}^{-\mathbf{k}_0,\mathrm{even},\dagger}(\mathbf{r}) \cdot \vec{\vec{\chi}}(\mathbf{r},\mathbf{r}_1,\mathbf{r}_2) \cdot \mathcal{L}_{\alpha_1}^{\mathbf{k}_1,\mathrm{odd}}(\mathbf{r}_1) \cdot \mathcal{L}_{\alpha_2}^{\mathbf{k}_2,\mathrm{even}}(\mathbf{r}_2) d^3\mathbf{r}\, d^3\mathbf{r}_1 d^3\mathbf{r}_2 \\
& + \int \mathcal{L}_{\alpha_0}^{-\mathbf{k}_0,\mathrm{odd},\dagger}(\mathbf{r}) \cdot \vec{\vec{\chi}}(\mathbf{r},\mathbf{r}_1,\mathbf{r}_2) \cdot \mathcal{L}_{\alpha_1}^{\mathbf{k}_1,\mathrm{even}}(\mathbf{r}_1) \cdot \mathcal{L}_{\alpha_2}^{\mathbf{k}_2,\mathrm{even}}(\mathbf{r}_2) d^3\mathbf{r}\, d^3\mathbf{r}_1 d^3\mathbf{r}_2 \\
& + i \int \mathcal{L}_{\alpha_0}^{-\mathbf{k}_0,\mathrm{even},\dagger}(\mathbf{r}) \cdot \vec{\vec{\chi}}(\mathbf{r},\mathbf{r}_1,\mathbf{r}_2) \cdot \mathcal{L}_{\alpha_1}^{\mathbf{k}_1,\mathrm{even}}(\mathbf{r}_1) \mathcal{L}_{\alpha_2}^{\mathbf{k}_2,\mathrm{even}}(\mathbf{r}_2) \times (-\mathbf{k}_0 \cdot \mathbf{r} + \mathbf{k}_1 \cdot \mathbf{r}_1 + \mathbf{k}_2 \cdot \mathbf{r}_2) d^3\mathbf{r}\, d^3\mathbf{r}_1 d^3\mathbf{r}_2.
\end{aligned} \tag{13}$$

For a centrosymmetric particle we have upon inversion of the spatial coordinates:

$$\vec{\vec{\chi}}(\mathbf{r},\mathbf{r}_1,\mathbf{r}_2) = -\vec{\vec{\chi}}(-\mathbf{r},-\mathbf{r}_1,-\mathbf{r}_2) \tag{14}$$

and for the local fields we have upon inversion,

$$\mathcal{L}_{\alpha_m}^{\mathbf{k},\mathrm{even}}(\mathbf{r}_m) = \mathcal{L}_{\alpha_m}^{-\mathbf{k},\mathrm{even}}(-\mathbf{r}_m) = \mathcal{L}_{\alpha_m}^{\mathbf{k},\mathrm{even}}(-\mathbf{r}_m), \tag{15}$$

$$\mathcal{L}_{\alpha_m}^{\mathbf{k},\mathrm{odd}}(\mathbf{r}_m) = \mathcal{L}_{\alpha_m}^{-\mathbf{k},\mathrm{odd}}(-\mathbf{r}_m) = -\mathcal{L}_{\alpha_m}^{\mathbf{k},\mathrm{odd}}(-\mathbf{r}_m). \tag{16}$$

Thus, for all second-order (and other even-order) nonlinear processes the leading order [Eq. (12)], vanishes since the contribution to the integral at $\{\mathbf{r},\mathbf{r}_1,\mathbf{r}_2\}$ is cancelled exactly by that at $\{-\mathbf{r},-\mathbf{r}_1,-\mathbf{r}_2\}$. The first nonvanishing terms are given by Eq. (13). For a noncentrosymmetric object (with a noncentrosymmetric shape or made of noncentrosymmetric material), Eq. (12) is the leading-order term.

In the limit of small scattering particles one can separate the properties of the scattering objects from the experimental geometry. In the zeroth-order approximation $\mathcal{L}_{\alpha}^{\mathbf{k},\mathrm{even}}$ is given by the electrostatic $(\mathbf{k}\to 0)$ approximation, which can be written as $\mathcal{L}_{\alpha}^{\mathbf{k},\mathrm{even}}(\mathbf{r}) \approx \vec{\vec{\mathcal{L}}}_{\mathrm{static}}(\mathbf{r}) \cdot \mathbf{u}_{\alpha}$ where $\mathcal{L}_{\mathrm{static}}(\mathbf{r})$ is a second-rank tensor. The next term, linear in $\mathbf{k}$, leads to a nonzero contribution: $\mathcal{L}_{\alpha}^{\mathbf{k},\mathrm{odd}}(\mathbf{r}) \approx \vec{\vec{\mathcal{M}}}(\mathbf{r}) : \mathbf{u}_{\alpha} \cdot \mathbf{k}$, where $\vec{\vec{\mathcal{M}}}$ is a third-rank tensor.

This separates the experimental geometry (contained in $\mathbf{k}$ and $\mathbf{u}_{\alpha}$) from the particle properties in the field factors. The omitted terms are of second or higher order in (σ/λ), which can be neglected for small particles. For small particles we can expand $\Gamma_{\alpha_0,\alpha_1,\alpha_2}^{\mathbf{k}_0,\mathbf{k}_1,\mathbf{k}_2}$ as

$$\begin{aligned}
\Gamma_{\alpha_0,\alpha_1,\alpha_2}^{\mathbf{k}_0,\mathbf{k}_1,\mathbf{k}_2} \approx & \vec{\vec{\Gamma}}_d \cdot \mathbf{u}_{\alpha_0} \cdot \mathbf{u}_{\alpha_1} \cdot \mathbf{u}_{\alpha_2} + \vec{\vec{\Gamma}}_{Q0} \cdot \mathbf{u}_{\alpha_0} \cdot \mathbf{k}_0 \cdot \mathbf{u}_{\alpha_1} \cdot \mathbf{u}_{\alpha_2} \\
& + \vec{\vec{\Gamma}}_{Q1} \cdot \mathbf{u}_{\alpha_0} \cdot \mathbf{u}_{\alpha_1} \cdot \mathbf{k}_1 \cdot \mathbf{u}_{\alpha_2} \\
& + \vec{\vec{\Gamma}}_{Q2} \cdot \mathbf{u}_{\alpha_0} \cdot \mathbf{u}_{\alpha_1} \cdot \mathbf{u}_{\alpha_2} \cdot \mathbf{k}_2,
\end{aligned} \tag{17}$$

where the third-rank $\vec{\vec{\Gamma}}_d$ and the forth-rank $\vec{\vec{\Gamma}}_Q$ tensors describe the dipole (d) and quadrupole (Q) contributions and depend on the properties of the scattering object only. For SHG scattering from small spheres the above expression has been evaluated previously by Dadap *et al.*[8]

B. Index matched particles

In Secs. III B and III C we consider nonlinear index-matched Rayleigh-Gans-Debye (RGD) and small contrast Wentzel-Kramers-Brillouin (WKB) scattering. From now on, we shall restrict ourselves to a local form of the second-order susceptibility, i.e., $\vec{\vec{\chi}}(\mathbf{r},\mathbf{r}_1,\mathbf{r}_2) = \boldsymbol{\chi}^{(2)}(\mathbf{r})\delta(\mathbf{r}-\mathbf{r}_1)\delta(\mathbf{r}-\mathbf{r}_2)$. Furthermore, we shall assume that the scattering particles are

made of centrosymmetric material so that $\boldsymbol{\chi}^{(2)}(\mathbf{r})$ is nonvanishing only at the particle surface. These assumptions are very common in nonlinear surface spectroscopy.[25] Equation (8) then takes the form of a surface integral,

$$\Gamma^{(2)}_{\alpha_0,\alpha_1,\alpha_2} = \oint \mathcal{L}^{-\mathbf{k}_0,\dagger}_{\alpha_0}(\mathbf{r}) \cdot \boldsymbol{\chi}^{(2)}(\mathbf{r}) \cdot \mathcal{L}^{\mathbf{k}_1}_{\alpha_1}(\mathbf{r}) \cdot \mathcal{L}^{\mathbf{k}_2}_{\alpha_2}(\mathbf{r}) e^{i(-\mathbf{k}_0+\mathbf{k}_1+\mathbf{k}_2)\cdot\mathbf{r}} d^2\mathbf{r}. \tag{18}$$

Before considering the cases of index matched and small index contrast scattering, we remark that the optical fields in the vicinity of an interface can be strongly screened by the surface. The local-field factors $\mathcal{L}^{\mathbf{k}}_{\alpha}$ depend on whether the fields are evaluated outside or inside the particle.[15] $\boldsymbol{\chi}^{(2)}$ appearing in Eq. (18) is an effective integrated nonlinear susceptibility, which must include the surface screening effects (that are intrinsically nonlocal). Consequently, the values of the elements of $\boldsymbol{\chi}^{(2)}$ depend on the definitions adopted. It is assumed in this work that the fields are evaluated at the outer side of the particle surface and the nonlinear source is located outside. Furthermore, Eq. (18) assumes that the curvature of the particle surface is small on the scale of the screening length so that the concept of the effective surface susceptibility[26] is applicable.

Equation (18) can be evaluated if the local field factors $\mathcal{L}^{\mathbf{k}}_{\alpha}$ are known. If the refractive index of the particle (n_p) and the surrounding medium (n_m) are matched, such that $|((n_p/n_m)-1)| \ll 1$, the local fields can be assumed to be identical to the incoming fields. This approximation is known as the Rayleigh-Gans-Debye approximation in which $\mathcal{L}_{\alpha}(\mathbf{r}) = \mathbf{u}_{\alpha}$.

The effective second-order polarizability can then be written as:

$$\Gamma^{(2)}_{\alpha_0,\alpha_1,\alpha_2}(\mathbf{q}) = \oint \mathbf{u}^{-\mathbf{k}_0,\dagger}_{\alpha_0}(\mathbf{r}) \cdot \boldsymbol{\chi}^{(2)}(\mathbf{r}) \cdot \mathbf{u}^{\mathbf{k}_1}_{\alpha_1}(\mathbf{r}) \cdot \mathbf{u}^{\mathbf{k}_2}_{\alpha_2}(\mathbf{r}) e^{i\mathbf{q}\cdot\mathbf{r}} d^2\mathbf{r} \tag{19}$$

with $\mathbf{q} = -\mathbf{k}_0 + \mathbf{k}_1 + \mathbf{k}_2 = q\hat{\mathbf{q}}$ the scattering wave vector. For an arbitrary particle shape we can now find the scattered field, Eq. (6), in terms of $\boldsymbol{\Gamma}^{(2)}$.

It is enlightening to draw an analogy between sum frequency scattering and conventional sum frequency generation from an (effective) planar surface.[26] We define this effective surface (lower panel of Fig. 2) to be orthogonal to the scattering wave vector $\mathbf{q}$ (illustrated in the top panel of Fig. 2). Thus, we can envisage the scattering particle as an effective surface with its normal (Z) parallel to $\mathbf{q}$. In sum frequency generation from a surface it is the interface that breaks the inversion symmetry, leading to a second-order nonlinear response. For a centrosymmetric index-matched particle it is the spatial variation of the phase factor $e^{i\mathbf{q}\cdot\mathbf{r}}$, which lifts the inversion symmetry. In this picture, $\boldsymbol{\Gamma}^{(2)}$ plays the role of the effective susceptibility of a surface. For a symmetric particle (similar to an isotropic surface) there are only four independent elements: $\Gamma^{(2)}_{\perp\perp\perp}$, $\Gamma^{(2)}_{\perp\parallel\parallel}$, $\Gamma^{(2)}_{\parallel\perp\parallel}$, and $\Gamma^{(2)}_{\parallel\parallel\perp}$, where $\perp$ refers to directions perpendicular to the effective surface (i.e., parallel to $\mathbf{q}$) and $\parallel$ refers to directions parallel to the effective surface. The solutions for the transverse scattered sum frequency fields become

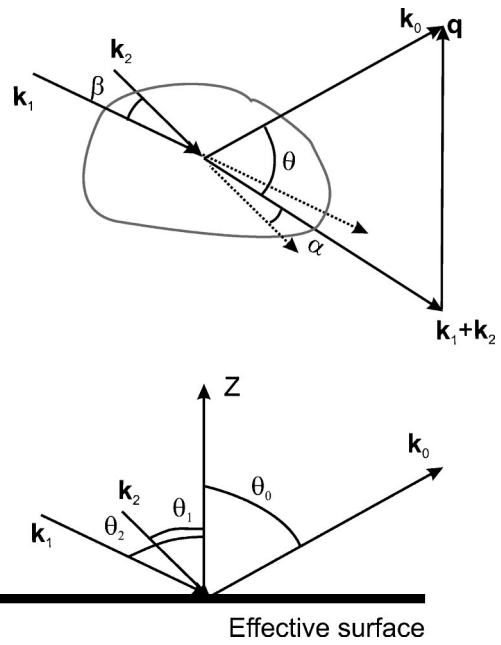

FIG. 2. Illustration of the analogy between a sum frequency scattering experiment and a surface sum frequency experiment in reflection mode from a planar surface. Top panel: Scattering geometry with relevant parameters. Bottom panel: Surface analogy.

$$E_{ppp}(r) = -\mathcal{E}^{\omega_1}\mathcal{E}^{\omega_2}\frac{\omega^2 e^{ik_0 r}}{2c^2 r}\left\{\cos\frac{\theta}{2}[(\Gamma^{(2)}_{\perp\perp\perp}+\Gamma^{(2)}_{\perp\parallel\parallel})\cos\beta + (\Gamma^{(2)}_{\perp\perp\perp}-\Gamma^{(2)}_{\perp\parallel\parallel})\cos(\theta-\beta+2\alpha)] - \sin\frac{\theta}{2}[(\Gamma^{(2)}_{\parallel\parallel\perp} - \Gamma^{(2)}_{\parallel\perp\parallel})\sin\beta + (\Gamma^{(2)}_{\parallel\perp\parallel}+\Gamma^{(2)}_{\parallel\parallel\perp})\sin(\theta-\beta+2\alpha)]\right\}, \tag{20}$$

$$E_{ssp}(r) = -\mathcal{E}^{\omega_1}\mathcal{E}^{\omega_2}\frac{\omega^2 e^{ik_0 r}}{2c^2 r}\Gamma^{(2)}_{\parallel\parallel\perp}\left(\cos\beta\cos\left(\frac{\theta}{2}+\alpha\right) + \sin\beta\sin\left(\frac{\theta}{2}+\alpha\right)\right), \tag{21}$$

$$E_{sps}(r) = -\mathcal{E}^{\omega_1}\mathcal{E}^{\omega_2}\frac{\omega^2 e^{ik_0 r}}{2c^2 r}\Gamma^{(2)}_{\parallel\perp\parallel}\cos\left(\frac{\theta}{2}+\alpha\right), \tag{22}$$

$$E_{pss}(r) = -\mathcal{E}^{\omega_1}\mathcal{E}^{\omega_2}\frac{\omega^2 e^{ik_0 r}}{2c^2 r}\Gamma^{(2)}_{\perp\parallel\parallel}\cos\left(\frac{\theta}{2}\right), \tag{23}$$

where θ is the scattering angle, α is the angle between $\mathbf{k}_1$ and $(\mathbf{k}_1+\mathbf{k}_2)$, β is the angle between $\mathbf{k}_1$ and $\mathbf{k}_2$, and $p(s)$ refers to polarization parallel (perpendicular) to the plane of incidence.

If we introduce angles $\theta_{0,1,2}$ as in Fig. 2 we can rewrite Eq. (20) as

$$\begin{aligned} E_{ppp}(\mathrm{r}) \propto 2(&\Gamma^{(2)}_{\perp\perp\perp} \sin\theta_0 \sin\theta_2 \sin\theta_1 \\ &+ \Gamma^{(2)}_{\perp\parallel\parallel} \sin\theta_0 \cos\theta_2 \cos\theta_1 \\ &- \Gamma^{(2)}_{\parallel\parallel\perp} \cos\theta_0 \cos\theta_2 \sin\theta_1 \\ &- \Gamma^{(2)}_{\parallel\perp\parallel} \cos\theta_0 \sin\theta_2 \cos\theta_1). \end{aligned} \tag{24}$$

Apart from a geometrical factor, this expression corresponds exactly to that found for a conventional surface sum frequency experiment (when the Fresnel factors[26] are neglected, which is essentially the Rayleigh-Gans-Debye approximation). The difference lies in the nature of the detection. In a surface sum frequency experiment one detects the whole SFG signal in the far field and has to take into account the illuminated area of the surface (resulting in an amplitude factor that scales with $1/\cos\theta_0$). In the scattering experiment only a small portion of the scattered field is collected, determined by the solid angle of detection.

For a given particle shape $\mathbf{\Gamma}^{(2)}$ can be expressed in terms of the local susceptibility elements, the scattering angle and particle dimension (both contained in $\mathbf{q}$). For an isotropic medium we only need to consider the surface contributions. For a spherical particle we can write

$$\Gamma^{(2)}_{ijk}(\mathbf{q}) = \sum_{\alpha,\beta,\gamma} \chi^{(2)}_{\alpha\beta\gamma} \oint (\mathbf{e}_\alpha \cdot \mathbf{u}_i)(\mathbf{e}_\beta \cdot \mathbf{u}_j)(\mathbf{e}_\gamma \cdot \mathbf{u}_k) e^{i\mathbf{q}\cdot\mathbf{r}} d^2\mathbf{r}, \tag{25}$$

where the integral is over the particle surface, $\chi^{(2)}_{\alpha\beta\gamma}$ are the elements of the local surface susceptibility, and $\mathbf{e}_{\alpha,\beta,\gamma}$ represent the unit vectors of the spherical coordinate system of the particle. The resulting expressions for the elements of $\mathbf{\Gamma}^{(2)}$ are given in Table I for an isotropic spherical particle (for which $\boldsymbol{\chi}^{(2)}$ has only four independent elements[1]).

C. Small index difference

One of the successful models, that has been used in the past to describe linear scattering, is the so-called Wentzel-Kramers-Brillouin (WKB) approximation.[27] It can be applied to particles, which have relatively small refractive index contrast ($\delta n = n_p - n_m$) with the surrounding medium, i.e., $|\delta n| \ll 1$. In the RGD approximation the electromagnetic wave is assumed to travel through the particle, without being modified in any way by its presence. It has been demonstrated that in linear scattering the most important refinement lies in the phase-shift that an electromagnetic wave experiences as it travels through the particle.[27] To embed this first correction in the RGD approximation, one can assume that the waves retain their parallel character, without changing direction or amplitude. Hence the phase on the directly illuminated half of the particle (the white area in Fig. 3) is exactly that of the incoming wave, whereas the phase of the outgoing wave (the grey area in Fig. 3) must be corrected by an amount $\delta n_i l_i k_i$, where δn_i is the refractive index contrast at the frequency of the ith wave, having wave vector $\mathbf{k_i}$ and l_i is the distance travelled by the wave inside the particle.

TABLE I. Values of the elements of the effective second-order polarizability $\mathbf{\Gamma}^{(2)}$ for sum frequency scattering from a sphere with radius σ, in terms of the local susceptibilities $\boldsymbol{\chi}^{(2)}$ and experimental observables,[9] θ and σ.

$\Gamma^{(2)}_{\perp\perp\perp}$	$2\pi(\mathrm{B}\chi^{(2)}_{\perp\perp\perp} + \mathrm{A}(\chi^{(2)}_{\perp\parallel\parallel} + \chi^{(2)}_{\parallel\perp\parallel} + \chi^{(2)}_{\parallel\parallel\perp}))$
$\Gamma^{(2)}_{\perp\parallel\parallel}$	$\pi(\mathrm{A}\chi^{(2)}_{\perp\perp\perp} + (\mathrm{A}+2\mathrm{B})\chi^{(2)}_{\perp\parallel\parallel} - \mathrm{A}(\chi^{(2)}_{\parallel\perp\parallel} + \chi^{(2)}_{\parallel\parallel\perp}))$
$\Gamma^{(2)}_{\parallel\perp\parallel}$	$\pi(\mathrm{A}(\chi^{(2)}_{\perp\perp\perp} - \chi^{(2)}_{\perp\parallel\parallel}) + (\mathrm{A}+2\mathrm{B})\chi^{(2)}_{\parallel\perp\parallel} - \mathrm{A}\chi^{(2)}_{\parallel\parallel\perp})$
$\Gamma^{(2)}_{\parallel\parallel\perp}$	$\pi(\mathrm{A}(\chi^{(2)}_{\perp\perp\perp} - \chi^{(2)}_{\perp\parallel\parallel}) - \mathrm{A}\chi^{(2)}_{\parallel\perp\parallel} + (\mathrm{A}+2\mathrm{B})\chi^{(2)}_{\parallel\parallel\perp})$
A	$(6i/q^4\sigma^2)\{2(1-q^2\sigma^2/3)\sin(q\sigma) - 2q\sigma\cos(q\sigma)\}$
B	$(6i/q^4\sigma^2)\{(q^2\sigma^2-2)\sin(q\sigma) - q\sigma(q^2\sigma^3/3-2)\cos(q\sigma)\}$

If we apply this to scattering by a spherical particle, the local field at the *outer side* of the surface can be written as

$$\mathcal{L}^{\mathbf{k}_i}_{\alpha_i}(\mathbf{r}) = \mathbf{u}^{\mathbf{k}_i}_{\alpha_i} \exp(i\delta n_i[\mathbf{k}_i \cdot \mathbf{r} + |\mathbf{k}_i \cdot \mathbf{r}|]). \tag{26}$$

Effectively this restates that the wave becomes phase shifted as it exits the sphere. Namely, for $\mathbf{k}_i \cdot \mathbf{r} < 0$ (on the illuminated part of the particle) the two terms in the exponent cancel each other and $\mathcal{L}^{\mathbf{k}_i}_{\alpha_i} \rightarrow \mathbf{u}^{\mathbf{k}_i}_{\alpha_i}$.

With the aid of Eq. (18) the effective surface polarizability of a sphere in the WKB approximation becomes

$$\begin{aligned} \Gamma^{(2)}_{\alpha_0,\alpha_1,\alpha_2} = \oint &[\mathbf{u}^{\mathbf{k}_0}_{\alpha_0} \cdot \boldsymbol{\chi}^{(2)}(\mathbf{r}) \cdot \mathbf{u}^{\mathbf{k}_1}_{\alpha_1} \cdot \mathbf{u}^{\mathbf{k}_2}_{\alpha_2}] \exp(-i\mathbf{q}\cdot\mathbf{r}) \\ &\times \exp[i\delta n_0(-\mathbf{k}_0 \cdot \mathbf{r} + |\mathbf{k}_0 \cdot \mathbf{r}|) + i\delta n_1(\mathbf{k}_1 \cdot \mathbf{r} \\ &+ |\mathbf{k}_1 \cdot \mathbf{r}|) + i\delta n_2(\mathbf{k}_2 \cdot \mathbf{r} + |\mathbf{k}_2 \cdot \mathbf{r}|)] d^2\mathbf{r}. \end{aligned} \tag{27}$$

For a centrosymmetric sphere one can also use the symmetry of $\chi^{(2)}$ upon inversion of the spatial coordinates, namely,

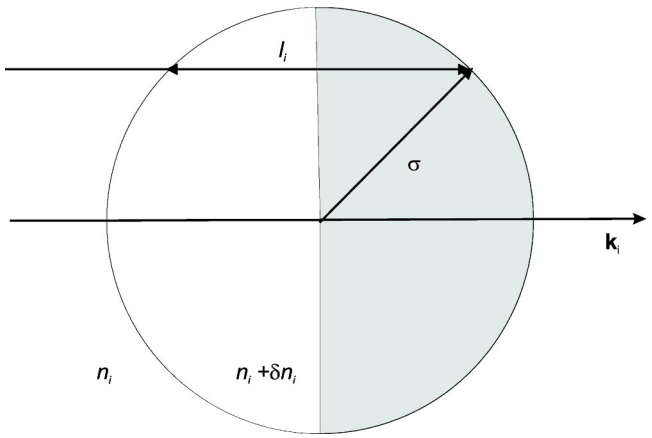

FIG. 3. Illustration of the Wentzel-Kramers-Brillouin approximation. At the surface of the backside (dark area) the wave is phase shifted.

$$\boldsymbol{\chi}^{(2)}(-\mathbf{r}) = -\boldsymbol{\chi}^{(2)}(\mathbf{r}).$$

The integral in Eq. (27) runs over the whole spherical surface and, thus, $\mathbf{r}$ can be replaced by $-\mathbf{r}$. We can rewrite the integral as a half of the sum of these two forms (i.e., with $\mathbf{r}$ and $-\mathbf{r}$). This gives

$$\Gamma^{(2)}_{\alpha_0,\alpha_1,\alpha_2} = i\oint \mathbf{u}^{\mathbf{k}_0}_{\alpha_0}\cdot\boldsymbol{\chi}^{(2)}(\mathbf{r})\cdot\mathbf{u}^{\mathbf{k}_1}_{\alpha_1}\cdot\mathbf{u}^{\mathbf{k}_2}_{\alpha_2}\exp(i\,\delta n_0|\mathbf{k}_0\cdot\mathbf{r}| + i\,\delta n_1|\mathbf{k}_1\cdot\mathbf{r}| + i\,\delta n_2|\mathbf{k}_2\cdot\mathbf{r}|)\sin(\mathbf{q}\cdot\mathbf{r} - \delta n_0\mathbf{k}_0\cdot\mathbf{r} + \delta n_1\mathbf{k}_1\cdot\mathbf{r} + \delta n_2\mathbf{k}_2\cdot\mathbf{r})d^2\mathbf{r}. \quad (28)$$

If we compare these expressions to the ones obtained using the RGD approximation it is clear that if the refractive index contrast δn_i becomes appreciable and frequency dependent $\delta n_0 \neq \delta n_1 \neq \delta n_2$, the scattered intensity in the phase matched direction ($\mathbf{q}=0$) is not necessarily 0.

D. Correlated scattering

So far, we have considered scattering from only one particle. In general, even the linear-optical problem of light interaction with scattering media consisting of many scatterers could be very complex and could include such effects as weak localization of light and coherent backscattering.[28,29] If scatterers are organized in a periodic structure, photonic band gaps can be opened.[30,31] Here, we restrict ourselves to much simpler situations when scattering is weak so that one can neglect the effect of the scatterers on the wave propagation (i.e., one can ignore multiple scattering of the incident waves). For a system of many scatterers one has to take into account the fact that the phases of the scattered waves can become correlated. In the following we assume that the sample consists of N identical particles, which are spherically symmetric, i.e., their scattering field does not depend on their orientation. Furthermore, it is supposed that (linear-optical) scattering is weak so that one can neglect the effect of the scatterers on the wave propagation (i.e., one can ignore multiple scattering of the scattered wave).

We then have to sum up all the scattered waves $\mathbf{E}_j$. Given the assumptions mentioned above, these fields have the same amplitude but may possess a different phase that arises from a position-dependent delay of the fundamental fields and the varying path length of the scattered fields (the distance between the scatterer and the detector, $|\mathbf{r}_0|$). In the Fraunhofer zone (i.e., $|\mathbf{r}_j-\mathbf{r}_k| \ll \sqrt{\lambda|\mathbf{r}_0|}$) we can write for the scattered intensity,

$$I(\mathbf{q}) = \sum_{k=1}^{N}\sum_{j=1}^{N}|\mathbf{E}|^2 e^{i\mathbf{q}(\mathbf{r}_j-\mathbf{r}_k)} = N|E|^2\left\langle \sum_{j=1}^{N} e^{i\mathbf{q}(\mathbf{r}_j-\mathbf{r}_k)}\right\rangle_k, \quad (29)$$

where the brackets denote an ensemble average. This bracketed term is known as the structure factor $S(\mathbf{q})$ in x-ray diffraction.[32,33] If the concentration of scattering particles is low there is no positional correlation between the emitted fields of the individual particles and the only nonzero contribution to the sum in Eq. (29) arises from terms with $j=k$. This means that we are dealing with independent scatterers and that the scattered intensity can be described by uncorrelated scattering, i.e., $S(\mathbf{q})=1$. Consequently, the total scattered intensity can be described by an incoherent sum of the scattered intensity of the individual particles. For a dense suspension, the particle positions become correlated, leading to correlations of the phases of the scattered fields, so that $S(\mathbf{q}) \neq 1$. In a disordered (fluid) suspension the structure factor $S(\mathbf{q})$ will reflect the short-range order between the neighbors, while if the particles form a regular periodic structure (as in colloidal crystals, for example), the long-range correlation between the particle positions leads to development of the Bragg peaks in $S(\mathbf{q})$ at specific values of the scattering vector $\mathbf{q}$.

Thus, the effect of particle correlations on nonlinear scattering is very similar to that in linear optics. However, an interesting aspect appears in the forward scattering, for $\mathbf{q}=0$. In linear scattering and diffraction extraction of useful information in the forward direction ($\mathbf{q}=0$) is complicated due to the presence of the strong primary beam. In contrast, this is not necessarily the case for nonlinear scattering as one can directly measure the scattered field in the forward direction. At $\mathbf{q}=0$ the waves scattered by different particles have the same phase, which should lead to a development of a Bragg-type forward peak even in disordered structures without long-range order. For periodic (crystalline) arrangements of scattering particles comparison of the "true" Bragg peaks (at $\mathbf{q}\neq 0$) and the forward peak (at $\mathbf{q}=0$) could open novel approaches to access information on e.g. long-range ordering from a nonlinear diffraction experiment.

As discussed above, the forward scattering intensity of a single particle could be very weak, which could complicate the observation of the forward nonlinear scattering peak. In the case of second harmonic generation ($\omega_1=\omega_2$) the intensity scattered exactly into the forward direction should vanish due to symmetry reasons. A forward SHG peak observed in Ref. 16 in transmission through a system of silicon nanoclusters in a silica matrix was associated with spatial inhomogeneities in the medium on length scales exceeding the wavelength or a gradient of the light intensity in a tightly focused laser beam.[17] Both explanations imply that the forward SHG peak must be broader than the angular width of the excitation beam, in agreement with experiment.[16] In the case of sum frequency generation ($\omega_1 \neq \omega_2$) with a noncollinear excitation geometry, however, the symmetry does not forbid forward scattering from a single particle even if the latter possesses spherical symmetry. As shown in the preceding section and further illustrated in Sec. V, the forward scattering intensity remains finite for a finite refractive index mismatch.

As a final remark, we note that for given directions of the fundamental beams, $\mathbf{q}$ can be finite for any detection direction since its length (given by $|\mathbf{q}|=|-\mathbf{k}_0+\mathbf{k}_1+\mathbf{k}_2|$) is determined by both the incidence angle and the refractive indices for each different wavelength. In this case the resulting intensity should depend on the sample thickness d in the direction at which $\mathbf{q}$ reaches its minimum value $\mathbf{q}_{\min}$. For $dq_{\min} \ll 1$ the whole sample volume will coherently contribute to the forward peak. Otherwise, for $dq_{\min} > 1$, the intensity of the forward scattering will display beatings as a function of the sample thickness d.

IV. EXPERIMENT

To test the theory presented above we have performed infrared-visible sum frequency scattering experiments on colloidal suspensions consisting of submicron particles. Information about the local environment on the particle surface can be obtained by analysis of both the spectrum and the angle dependence of the spectral features. From the spectrum information about the local structure can be obtained, as the absence or presence of local inversion symmetry leads to distinct spectral features.[9] The angle resolved data can be used to extract information about the orientation. The sum frequency scattering experiments were performed using 10 μJ (120 fs) infrared (IR) pulses (repetition rate 1 kHz, FWHM bandwidth of $\sim$180 cm^{-1}) centered around 2900 cm^{-1} and 3.0 μJ, 800 nm visible (VIS) pulses with a 10 cm^{-1} bandwidth. The selectively polarized IR and VIS pulses were incident under a relative angle of 15°(β) and were focused down to a $\sim$0.4 mm beamwaist. Note that the beam diameter at the focus is three orders of magnitude larger than the particle radius, so that field inhomogeneities across single particles are negligible.[16,17] The scattered light was collimated with a lens, polarization selected and dispersed onto a gated, intensified charge coupled device (CCD) camera.[34,35] The angular resolution was controlled by an aperture placed in front of the collimating lens and was typically 12°. The samples consist of dry stearic alcohol ($C_{18}H_{37}OH$) coated[36] silica particles[37] dispersed in CCl_4 (99.9%, Baker Analyzed) with radii (σ) of 342 nm, 123 nm, and 69 nm. The colloid volume fractions where, respectively, 5% (σ=342 nm), 4% (σ=123 nm), and 6.7% (σ=69 nm). The sample cell consists of 2 CaF_2 plates separated by a 1 mm Teflon spacer.

V. RESULTS AND DISCUSSION

Figure 4 shows SFG spectra of stearyl-coated silica particles with radii of 69 nm, 123 nm, and 342 nm, respectively. Only two (*ppp* and *ssp*) polarization combinations are shown (top panel). The intensity ratio is very well reproduced by the RGD theory as witnessed by the bottom panel, which shows calculated scattered power over a solid angle of 12° (marked by the shaded area). The solid lines in Fig. 4 are fits to the data, obtained by convoluting the effective susceptibility $\Gamma_n^{(2)}(\omega_1)$ with the electric field envelope of the upconversion pulse $E(\omega_2)$,[9,25,38,39]

$$I_0(\omega_1+\omega_2) \propto \left| \sum_n \Gamma_n^{(2)}(\omega_1) \otimes E(\omega_2) \right|^2,$$

$$\Gamma_n^{(2)}(\omega_1) = \frac{A_n}{(\omega_1-\omega_{0n})+i\Upsilon_n}, \tag{30}$$

where n refers to a vibrational mode, ω_{0n} is the resonance frequency, and Υ_n the spectral half width at half maximum. The fits were obtained using all five well-known CH stretch resonances:[40] the symmetric CH_3 and CH_2 stretches at 2890 cm^{-1} and 2853 cm^{-1}, the asymmetric CH_3 and CH_2 stretches at 2980 cm^{-1} and 2910 cm^{-1} and a Fermi resonance

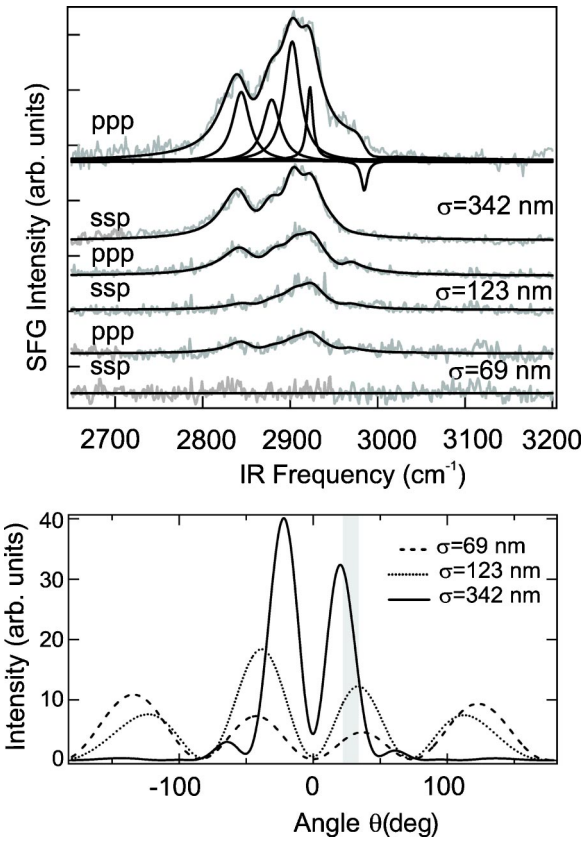

FIG. 4. Top panel: SFG spectra (gray lines) and fits (black lines) obtained at different polarization conditions (the three letter codes next to the spectra indicate polarizations (*p* for horizontal, *s* for vertical with respect to the plane of incidence for SFG, VIS, and IR, respectively) at a scattering angle of 26°. The angular resolution was 12°. The intensities are corrected for polarization dependent detector sensitivity. The solid lines are fits as described in the text. Bottom panel: Calculated intensities as a function of scattering angle. The shaded area indicates the angle for which the spectra in the top panel have been recorded.

at 2930 cm^{-1}. The central frequencies were obtained from a linear infrared spectrum and a Raman spectrum of the same colloid sample. This fit procedure is justified, because for a given scattering angle, the transverse component of the scattered field is a linear combination of the components of the effective nonlinear spherical polarizability $\mathbf{\Gamma}^{(2)}$.[9]

Figure 5 shows the scattered intensity for the symmetrical CH_3 stretch vibration ($|A_{\mathrm{sym.CH_3}}|^2$) of the stearyl groups attached to the surface of the 342 nm and the 123 nm particles as a function of the scattering angle θ. As the contrast between the particles and the solvent is relatively small, we see that the RGD approximations provides a good description of the scattered field. Both fits were generated with the same values for the elements of the susceptibility tensor, namely, $\chi^{(2)}_{\perp\parallel\parallel}/\chi^{(2)}_{\perp\perp\perp}=-0.29$, $\chi^{(2)}_{\parallel\perp\parallel}/\chi^{(2)}_{\perp\perp\perp}=0.28$, and $\chi^{(2)}_{\parallel\parallel\perp}/\chi^{(2)}_{\perp\perp\perp}=0.32$. Figure 6 shows a comparison between the RGD and WKB approximations. Angular distributions are calculated for different radii. The input parameters are: $\chi^{(2)}_{\perp\perp\perp}=1$, $\chi^{(2)}_{\perp\parallel\parallel}=0$, $\chi^{(2)}_{\parallel\perp\parallel}=0$, $\chi^{(2)}_{\parallel\parallel\perp}=0$, and $\lambda_1=3448$ nm, $n_1=1.49$, $\lambda_2=793$ nm, $n_2=1.46$, $\lambda_0=645$ nm, $n_0=1.46$ and a realistic re-

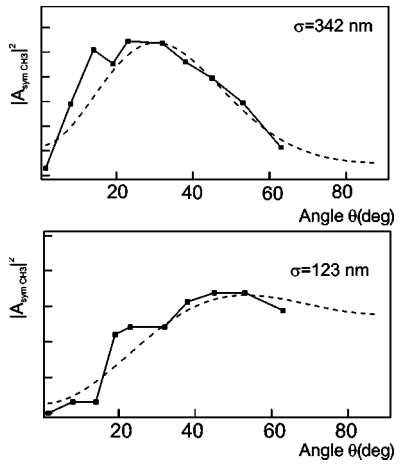

FIG. 5. The angular distribution of SFG intensity for the symmetrical CH_3 stretch mode for silica particles with $\sigma=342$ nm (top panel) and $\sigma=123$ nm (bottom panel). The dashed lines are fits to the data using Eq. (20).

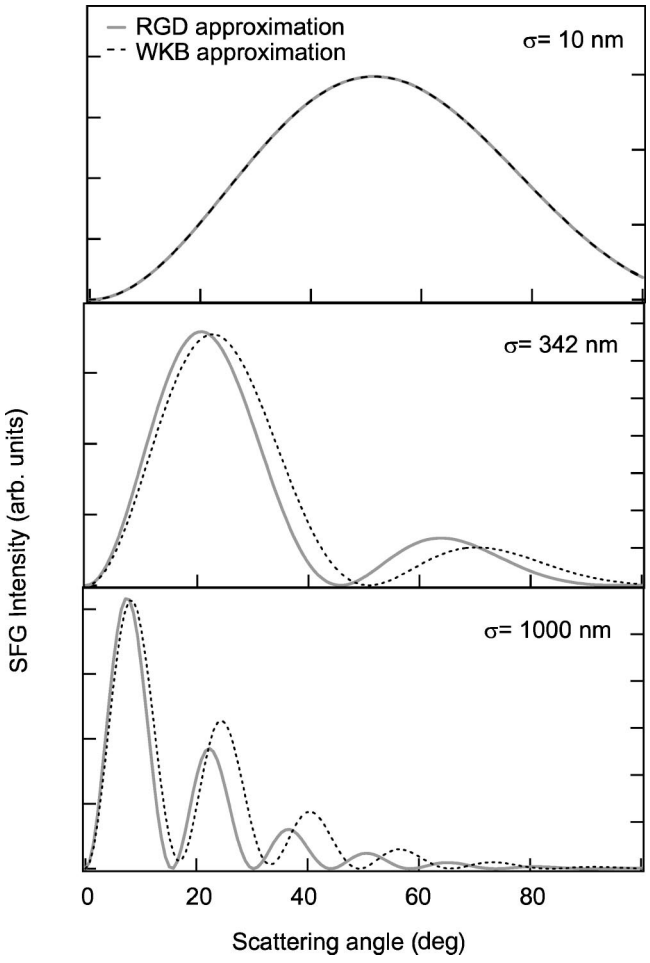

FIG. 6. Comparison of the Wentzel-Kramers-Brillouin approximation to the Rayleigh Gans Debye approximation for spherical particles, with a radius of 10 nm, 342 nm, and 1000 nm. It shows that for larger particles the phase shift becomes significant and the scattering patterns start to differ.

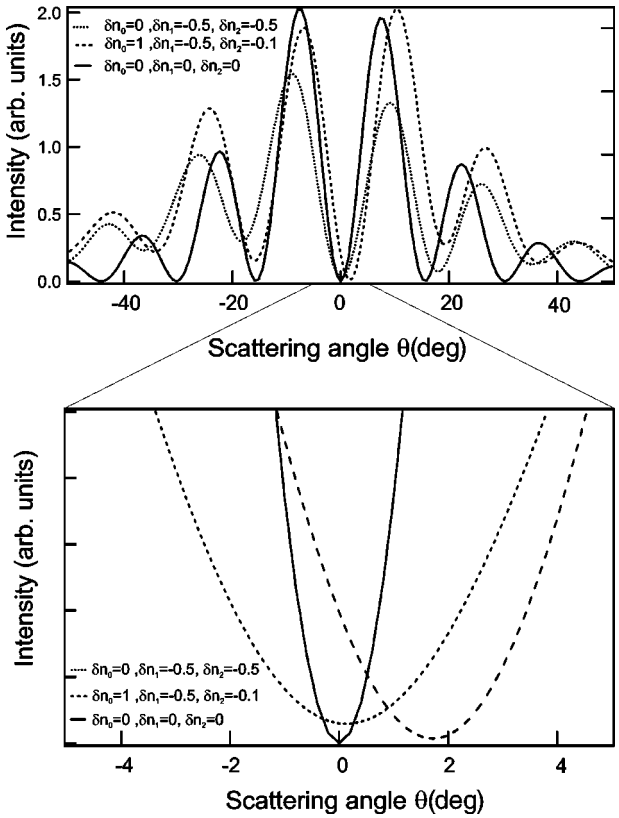

FIG. 7. Scattered intensity for a single sphere with a radius of 1000 nm in the Wentzel-Kramer-Brilliouin approximation, with different values of $\delta n_{0,1,2}$, demonstrating that in contrast to the Rayleigh-Gans-Debye approximation ($\delta n_{0,1,2}=0$) there can be scattered intensity in the phasematched direction if the index contrast increases.

fractive index contrast of $\delta n_i=-0.1$ (defined as the difference between the solute and the particle). For these values both approximations produce the same radiation pattern for the small (10 nm) particles. For larger sizes, the phase shift becomes significant and the scattering patterns start to differ. For relatively large particles (1 μm) the difference becomes appreciable, especially at larger angles. This effect was also observed when the RGD and WKB approximation were compared in linear scattering experiments.[27] This shows that for samples like the stearyl-coated silica particles in CCl_4 the Rayleigh-Gans-Debye approximation is valid and that typically for micron sized particles one needs to take into account the phase shift that the waves experience as they travel through the particle.

Figure 7 shows several calculations for the scattered SFG intensity as a function of the scattering angle for several refractive index contrasts. It shows that, in contrast to the Rayleigh-Gans-Debye approximation there can be scattered intensity in the phase matched direction if the index contrast increases. If we also take into account the notion that at this scattering angle the scattered intensity becomes proportional to the square of the number of particles in the suspension, we might expect a peak in the phase matched direction. In our experiments with colloidal particles dispersed in CCl_4 however, we were not able to observe a peak in this direction.

This could be due to the small contrast in our sample ($|\delta n| < 0.1$ for all wavelengths[9]) in combination with the relatively small radii. For a dried (drop-casted) sample of colloids we did observe a small signal in the forward direction. Due to a poor resolution we were not able to collect an angular dependent intensity plot. It does, however, corroborate our predictions.

VI. CONCLUSIONS

In conclusion, we have introduced the concept of an effective susceptibility to formulate a generalized treatment of nonlinear optical scattering. From simple symmetry arguments we can deduce selection rules that are independent of the properties of the scattering object. For sum frequency scattering in particular, we have considered limiting cases of small particle scattering, index matched (Rayleigh-Gans-Debye) scattering, small index contrast (Wentzel-Kramers-Brillouin) scattering and correlated scattering. We have compared these results to data from sum frequency scattering experiments and found that for particles with radii up to several hundred nanometers the RGD approximation generates a good description. Phase differences upon traversing the particle need to be incorporated for larger particles (for comparable refractive index contrast).

ACKNOWLEDGMENTS

The authors would like to thank M. Pronk, R. C. V. van Schie, and P. Schakel for excellent technical support, A. W. Kleyn, J. E. G. J Wijnhoven, and H. N. W. Lekkerkerker for many helpful discussions and J. I. Dadap, J. Shan, and T. F. Heinz for sharing unpublished work. This work is part of the research program of the Foundation for Fundamental Research on Matter (FOM), which is financially supported by the Netherlands Organization for Scientific Research (NWO).

*Electronic address: roke@chem.leidenuniv.nl

[1] Y. R. Shen, *The Principles of Nonlinear Optics* (Wiley, New York, 1984).
[2] R. W. Boyd, *Nonlinear Optics* (Academic, New York, 1992).
[3] T. Kikteva, D. Star, A. M. D. Lee, G. W. Leach, and J. M. Papanikolas, Phys. Rev. Lett. **85**, 1906 (2000).
[4] U. Hofer, Appl. Phys. B: Lasers Opt. **68**, 383 (1999).
[5] Ch. Hess, M. Bonn, S. Funk, and M. Wolf, Chem. Phys. Lett. **327**, 448 (2000).
[6] Ch. Hess, M. Wolf, and M. Bonn, Phys. Rev. Lett. **85**, 4341 (2000).
[7] G. Ma and H. C. Allen, J. Am. Chem. Soc. **124**, 9374 (2001).
[8] J. I. Dadap, J. Shan, K. B. Eisenthal, and T. F. Heinz, Phys. Rev. Lett. **83**, 4045 (1999).
[9] S. Roke, W. G. Roeterdink, J. E. G. J Wijnhoven, A. V. Petukhov, A. W. Kleyn, and M. Bonn, Phys. Rev. Lett. **91**, 258302 (2003).
[10] N. Yang, W. E. Angerer, and A. G. Yodh, Phys. Rev. Lett. **87**, 103902 (2001).
[11] J. I. Dadap, J. Shan, and T. F. Heinz, J. Opt. Soc. Am. B **21**, 1328 (2004).
[12] J. P. Dewitz, J. P. Hübner, and K. H. Bennemann, Z. Phys. D: At., Mol. Clusters **37**, 75 (1996).
[13] X. M. Hua and J. I. Gersten, Phys. Rev. B **33**, 3756 (1986).
[14] J. Martorell, R. Vilaseca, and R. Corbalán, Phys. Rev. A **55**, 4520 (1997).
[15] C. K. Chen, T. F. Heinz, D. Ricard, and Y. R. Shen, Phys. Rev. B **27**, 1965 (1983).
[16] Y. Jiang, P. T. Wilson, M. C. Downer, C. W. White, and S. P. Withrow, Appl. Phys. Lett. **78**, 766 (2001).
[17] W. L. Mochán, J. A. Maytorena, B. S. Mendoza, and V. L. Brudny, Phys. Rev. B **68**, 085318 (2003).
[18] J. D. Jackson, *Classical Electrodynamics* (Wiley, New York, 1975).
[19] L. D. Landau and E. M. Lifshitz, *Electrodynamics of Continuous Media* (Pergamon, Oxford, 1960).
[20] V. N. Gridnev, Phys. Rev. B **51**, 13 079 (1995).
[21] A. L. Shelankov and G. E. Pikus, Phys. Rev. B **46**, 3326 (1992).
[22] V. N. Gridnev, Solid State Commun. **100**, 71 (1996).
[23] A. V. Petukhov, V. L. Brudny, W. L. Mochán, J. A. Maytorena, B. S. Mendoza, and T. Rasing, Phys. Rev. Lett. **81**, 566 (1998).
[24] K. Sato, A. Kodama, M. Miyamoto, A. V. Petukhov, K. Takanashi, S. Mitani, H. Fujimori, A. Kirilyuk, and Th. Rasing, Phys. Rev. B **64**, 184427 (2001).
[25] T. F. Heinz, *Nonlinear Surface Electromagnetic Phenomena* (Elsevier, New York, 1991), Chap. 5.
[26] A. V. Petukhov, Phys. Rev. B **52**, 16 901 (1995).
[27] D. Deirmandjian, Ann. Geophys. (C.N.R.S.) **13**, 286 (1957).
[28] D. S. Wiersma, P. Bartoliniand, A. Lagendijk, and R. Righini, Nature (London) **390**, 671 (1997).
[29] R. Sapienza, S. Mujumdar, C. Cheung, A. G. Yodh, and D. Wiersma, Phys. Rev. Lett. **92**, 033903 (2004).
[30] E. Yablonovitch, Phys. Rev. Lett. **58**, 2059 (1987).
[31] J. E. G. J. Wijnhoven and W. L. Vos, Science **281**, 802 (1998).
[32] C. Kittel, *Introduction to Solid State Physics* (Wiley, New York, 1996).
[33] A. V. Petukhov, D. G. A. L. Aarts, I. P. Dolbnya, E. H. A. de Hoog, K. Kassapidou, G. J. Vroege, W. Bras, and H. N. W. Lekkerkerker, Phys. Rev. Lett. **88**, 208301 (2002).
[34] E. W. M. van der Ham, Q. H. F. Vrehen, and E. R. Eliel, Surf. Sci. **386**, 96 (1996).
[35] L. J. Richter, T. P. Petralli-Mallow, and J. C. Stephenson, Opt. Lett. **23**, 1594 (1998).
[36] A. van Helden, J. Jansen, and A. Vrij, J. Colloid Interface Sci. **81**, 354 (1981).
[37] W. Stöber, A. Vink, and R. Bohn, J. Colloid Interface Sci. **26**, 62 (1968).
[38] J. H. Hunt, P. Guyot-Sionnest, and Y. R. Shen, Chem. Phys. Lett. **133**, 189 (1987).
[39] S. Roke, J. M. Schins, M. Müller, and M. Bonn, Phys. Rev. Lett. **90**, 128101 (2003).
[40] X. Zhuang, P. B. Miranda, D. Kim, and Y. R. Shen, Phys. Rev. B **59**, 12 632 (1999).